JACS
JOURNAL OF THE AMERICAN CHEMICAL SOCIETY
Article
pubs.acs.org/JACS

Ionic Aggregate Structure in Ionomer Melts: Effect of Molecular Architecture on Aggregates and the Ionomer Peak

Lisa M. Hall,*[,†] Michelle E. Seitz,[‡,⊥] Karen I. Winey,[‡,¶] Kathleen L. Opper,[§,#] Kenneth B. Wagener,[§] Mark J. Stevens,[†,∥] and Amalie L. Frischknecht*[,†,∥]

[†]Computational Materials Science and Engineering Department and [∥]Center for Integrated Nanotechnologies, Sandia National Laboratories, Albuquerque, New Mexico 87185, United States

[‡]Department of Materials Science and Engineering and [¶]Department of Chemical and Biomolecular Engineering, University of Pennsylvania, Philadelphia, Pennsylvania 19104, United States

[§]Department of Chemistry, University of Florida, Gainesville, Florida 32611, United States

Supporting Information

ABSTRACT: We perform a comprehensive set of coarse-grained molecular dynamics simulations of ionomer melts with varying polymer architectures and compare the results to experiments in order to understand ionic aggregation on a molecular level. The model ionomers contain periodically or randomly spaced charged beads, placed either within or pendant to the polymer backbone, with the counterions treated explicitly. The ionic aggregate structure was determined as a function of the spacing of charged beads and also depends on whether the charged beads are in the polymer backbone or pendant to the backbone. The low wavevector ionomer peak in the counterion scattering is observed for all systems, and it is sharpest for ionomers with periodically spaced pendant charged beads with a large spacing between charged beads. Changing to a random or a shorter spacing moves the peak to lower wavevector. We present new experimental X-ray scattering data on Na^+-neutralized poly(ethylene-*co*-acrylic acid) ionomers that show the same two trends in the ionomer peak, for similarly structured ionomers. The order within and between aggregates, and how this relates to various models used to fit the ionomer peak, is quantified and discussed.

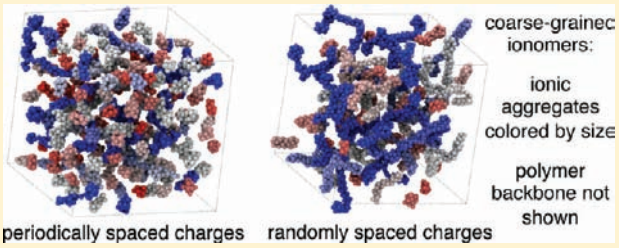

INTRODUCTION

Ionomer melts are polymers with a small fraction of charged groups and no solvent, which have been identified as possible battery electrolytes. Since the ionic groups (anions in this paper) are bound to the chain, they cannot collect at the electrode and interfere with the desired cation transport as can anions in conventional electrolytes. However, currently available ionomers are not conductive enough for battery applications. Because the ions exist in a relatively low dielectric polymer medium, their strong ionic attractions typically lead to ionic aggregation. The ionic aggregates act as temporary cross-links and lead to interesting mechanical properties but may hinder counterion transport. A molecular-level understanding of ionic aggregation and counterion dynamics, and their dependence on controllable ionomer characteristics such as polymer architecture, is needed to enable rational design of conducting ionomers.

Ionic aggregate morphology is likely a key driver of both mechanical and electrical properties but is difficult to explore in detail experimentally. A common way to experimentally assess ionic aggregate size and order is by measuring the low wavevector peak in the X-ray scattering, caused by the aggregates. The peak, called the "ionomer peak", is typical of many ionomers of widely varying chemistries.[1] It is often fit with the Yarusso–Cooper (YC) model or its more recent version, the Kinning–Thomas (KT) model.[1−5] These models propose that spherical regions of increased ion density (the aggregates) order like liquid-phase hard spheres with a radius of closest approach that is larger than the ion dense regions themselves, presumably due to steric hindrance from the uncharged polymer associated with the aggregate. To either bolster or refute the hypothesis of spherical aggregates for a given system, scanning transmission electron microscopy (STEM) can be used, but typically an image shows a 2D projection of many overlapping aggregates.[3,6−12] A microscopic 3D picture of ionic aggregate morphology which can show liquid-like interaggregate order can presently only be obtained in simulations. A major goal of the present work is to build a clearer description of the various ionic aggregate morphologies possible in simple dry ionomers and to relate morphology to experimental scattering signatures.

Many important theoretical insights into aggregation, or clustering, in polymer melts have already been made by considering polymers with a small number of strongly associating groups.[13−18] The attraction between such groups,

Received: September 28, 2011
Published: December 1, 2011

   dx.doi.org/10.1021/ja209142b | J. Am. Chem.Soc. 2012, 134, 574−587

called stickers, may represent a screened ionic interaction or strong chemical attraction such as hydrogen bonding. The attraction is relatively short-ranged, which simplifies its use in some theories and speeds up simulations versus long-range Coulomb interactions. Typically, all stickers are attracted to all other stickers, and there are no same-charge-like repulsive interactions or "counterions" (although it is possible to treat explicit counterions in certain theories of associating polymers, and some initial calculations have been done).[18] Associating polymer studies are relevant to ionic aggregation in ionomers because they consider the basic effects of strong enthalpic interactions in the presence of polymer backbone connectivity and entropic effects. However, the positive and negative charges in ionomers can produce a local structure of alternating charges, which is not reproduced by associating polymer models.

Both linear polymers with stickers on the ends of the chain (telechelics) and those with regularly spaced stickers in the chain have been studied. Nyrkova and co-workers discussed how clusters in ionomers are analogous to microdomains in block copolymers composed of alternating nonattractive and very short attractive blocks in what they define as the superstrong segregation regime.[15] Their free energy analysis predicted that telechelics form the largest clusters and that stickers placed randomly in the chain also form larger clusters than periodically placed stickers. Further work suggested that disk-shaped clusters may be preferred over spherical clusters.[14] The polymer reference interaction site model has also been applied to associating telechelic and periodically spaced associating polymers.[16−18] Both types formed dense clusters of associating groups at low enough temperatures, and telechelics clustered more strongly than the in-chain associating groups. Intercluster liquid-like order was predicted. Molecular dynamics (MD) simulations were performed on both melts and thin films of telechelic and in-chain associating polymers. Both types formed discrete, roughly spherical clusters, but again telechelics formed stronger and larger clusters.[13]

Including both long-range Coulombic interactions and free counterions in the dry ionomer model is crucial to understanding the detailed ionic aggregation behavior and charge transport for battery applications. We note that most prior simulations of ionomers including Coulomb interactions have focused on hydrated ionomers for fuel cell applications, which can form proton-conducting water channels.[19,20] Different types of network structures, based on different polymer chemistries and architectures, are possible and lead to different properties.[21] It remains unclear what parallels can be drawn between water-filled channels lined by ionic groups and dry, purely ionic aggregates. Water is typically avoided in batteries, and we discuss only dry ionomers in this paper. One group did study a dry fuel cell membrane material with permanently bound hydrogens (and no free counterions).[22]

A few coarse-grained MD simulations including explicit counterions have also been performed. Goswami et al. studied telechelic ionomers[23] and found disk-like ionic aggregates at low temperature. Based on the associating polymer work showing stronger aggregation in telechelics and because telechelics typically have a low fraction of ionic groups, periodically or randomly spaced ionomers seem more likely candidates for battery applications. Early simulations of ionomers with periodically spaced charged beads in the chain backbone (ionenes) showed the ions apparently percolated through the small simulation box at low temperatures.[24]

In previous work,[25] we performed coarse-grained MD simulations with two different ionomer architectures: periodically spaced ionenes and ionomers with charged beads placed pendant to the polymer backbone (pendants). The ionene system formed a percolated ionic structure at low dielectric constant, while the pendant ionomers instead formed discrete, roughly spherical aggregates. Only one periodic spacing was considered. The system size was large enough to resolve the average aggregate size and interaggregate ordering.[25] Both pendants and ionenes showed a significant ionomer scattering peak, although it was much more intense for pendants. For the pendant architecture, the aggregates' center-of-mass to center-of-mass structure factor revealed liquid-like interaggregate ordering corresponding to the ionomer scattering peak, as proposed by YC-type models. Increasing the dielectric constant was shown to decrease the aggregate size and the local and long-range order. We concluded that our coarse-grained model captures the most important aspects of ionomer physics leading to the ionomer peak, and that a small change in architecture can yield qualitatively different ionic aggregate morphologies.

Recent experimental advances have allowed synthesis and extensive characterization of similar ionomers with a variable precise or random spacing of ions along the chain.[4,26] The precise materials have a much stronger ionomer scattering peak than randomly spaced analogues, indicating a high degree of interaggregate order, and analysis of STEM micrographs suggests the aggregates are discrete spheres.[4,26] Such simply constructed and highly ordered materials are ideal for clear comparisons with simulations, and these experiments partially motivated both our prior work and this study.

In this paper, we present new precise and random Na^+-neutralized poly(ethylene-*co*-acrylic acid) (PEAA) ionomer X-ray scattering data and compare these to simulated structure factors. Having studied the effect of dielectric constant in prior work, here we focus on the effects on ionic aggregate morphology of (1) varying the spacing between charges and (2) randomness in the spacing. To better understand the range of possible ionic aggregate morphologies and their relationship with scattering profiles, we simulate both ionene and pendant architectures and add randomness in spacing in two different ways. The pendant ionomers' structure factors compare favorably with experimental scattering profiles: both show that increasing the spacing of periodic ionomers moves the ionomer peak to a lower wavevector, and that adding sequence randomness broadens the peak and also moves it to a lower wavevector. We first summarize the experimental and simulation methods. The Results section details our real-space and then Fourier-space structural results, including specific comparisons between the simulated and experimental ionomer peaks. The Discussion section explains the results further in the context of prior theoretical and experimental work.

EXPERIMENTAL METHODS

Materials. Linear PEAA copolymers with either precise or pseudorandom acid spacing were synthesized via ADMET and ROMP techniques, respectively. Details of their synthesis and characterization have been previously described.[26] They are shown schematically in Figure 1. We denote these polymers p9AA, p15AA, and r15AA to explain the placement of the acetic acid (AA) groups; these names start with a p to denote precise or an r for pseudorandom spacing, then have the number 9 or 15 to denote the average number of backbone carbons per COOH group. The neutralized samples discussed below are further denoted with -Y%Na, where Y is the mol

dx.doi.org/10.1021/ja209142b | J. Am. Chem.Soc. 2012, 134, 574−587

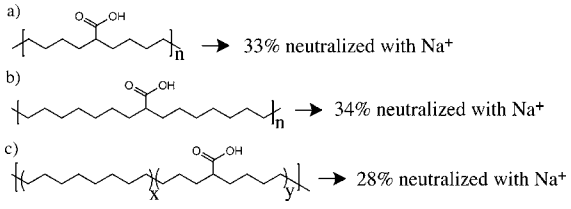

Figure 1. The three experimental polymers before neutralization and the percent of COOH groups that were neutralized: (a) p9AA, (b) p15AA, and (c) r15AA, where x/y = 0.88.

% neutralization determined from elemental analysis as given in Figure 1, and Na is the counterion label.

General Neutralization Procedure. The same solvent system was used to solubilize each PEAA acid polymer. Similar precipitation neutralization procedures were followed, yielding similar observations for all sodium ionomers. With p9AA (polymer a in Figure 1) as the representative example, in a dry single-neck round-bottom flask the p9AA was weighed (50 mg, 0.29 mmol), sealed with a septum, and dissolved with a 1:4 mixture of 1,4-dioxane and 1-butanol (15 mL) under nitrogen. A magnetic stir bar was added, and complete dissolution was obtained upon heating at 90 °C for 3 h. During that time, the sodium acetate salt (12 mg, 0.15 mmol) was weighed under a dry and inert atmosphere and then dissolved in a 1:2 mixture of 1,4-dioxane and 1-butanol (7.5 mL). For complete dissolution, a small stir bar was added and the vial was closed prior to heating to 90 °C for 30 min. The round-bottom flask was then outfitted with an addition funnel. The salt solution was added to the addition funnel and added dropwise into the vigorously stirring polymer solution at 90 °C. Cloudiness was observed upon partial addition. After the solution was stirred for 3 h at 90 °C and cooled to room temperature, the fine precipitate coagulated into larger pieces. The sodium ionomer slurry was cooled on ice prior to filtration of polymer p9AA-33%Na. The precipitate was filtered and dried at 80 °C overnight. The extent of neutralization achieved from the solution neutralization procedure was determined by inductively coupled plasma elemental analysis performed by Galbraith Laboratories (Knoxville, TN) on samples with masses ranging from 5 to 21 mg. The error is estimated at ~7% in the reported mol % neutralization.

X-ray Scattering. The samples were melt-pressed at 150 °C between sheets of polytetrafluoroethylene in a Carver 4122 hot press. Pressing resulted in the formation of uniform films for all samples. All samples were subjected to rapid cooling (~8 °C/min) in the press by flowing tap water. For X-ray scattering studies, samples were loaded into 1.0 mm diameter glass capillaries (Charles Supper Co. Special Glass 10-SG) which were then flame-sealed. The X-ray scattering apparatus consists of a Nonius FR591 rotating-anode generator operated at 40 kV × 85 mA, pinhole focusing optics, an evacuated flight path, and a Bruker HiSTAR multiwire two-dimensional detector. Data were acquired at a sample−detector distance of 7 cm, corresponding to a k range of ~2−18 nm^{-1} (we denote wavevector as k throughout this paper; experimentally, $k = (4\pi/\lambda)\sin\theta$). 2D data reduction, analysis, and curve fitting were performed using Datasqueeze software.[27] Sample-filled capillaries were loaded into a Linkham oven, and the temperature was controlled via a Linkham TMS 94 temperature controller. Samples were heated at 10 °C/min from room temperature to 118 °C and held at least 5 min prior to data collection to ensure thermal equilibrium was achieved. Data were collected for 1 h. An empty capillary was run under the same conditions and used for background subtraction. Distance calibration was done using silver behenate. Near the edge of the detector there is ~5% error in the peak position; therefore, the absolute peak positions have some distortion, but the relative shifting between samples is reliable.

SIMULATION METHODS

We use the coarse-grained bead−spring polymer model of Kremer and Grest.[28] Adjacent polymer beads are bonded by the finitely extensible nonlinear elastic (FENE) potential with a spring constant of $k = 30\varepsilon/\sigma^2$ and maximum extent of $R_0 = 1.5\sigma$:[28,29]

$$U_{\mathrm{FENE}}(r) = -0.5kR_0^2 \ln(1 - r^2/R_0^2) \quad (1)$$

A variable number of charged beads are placed either within the linear polymer backbone (as in Figure 2d) or pendant to a backbone bead (as in Figure 2a); we call these types of polymers "ionenes" and "pendants", respectively. An equal (neutralizing) number of counterions of opposite charge are explicitly added. All polymer beads and counterions interact with the repulsive part of the Lennard-Jones (LJ) potential, with $\varepsilon_{\mathrm{LJ}} = 1.0$, shifted to zero at its minimum:

$$U_{\mathrm{LJ}}(r) = \begin{cases} 4\varepsilon_{\mathrm{LJ}}\left[\left(\frac{\sigma_{\mathrm{LJ}}}{r}\right)^{12} - \left(\frac{\sigma_{\mathrm{LJ}}}{r}\right)^{6} + \frac{1}{4}\right]; & r \le r_c \\ 0; & r > r_c \end{cases} \quad (2)$$

where σ_{LJ} is the LJ diameter, $\varepsilon_{\mathrm{LJ}} = 1.0$ is the LJ unit of energy, r is the distance between two beads, and the cutoff distance $r_c = 2^{1/6}\sigma$. The LJ diameter of all polymer beads is $\sigma = 1.0$, the distance unit in which we report most of our results. Most systems studied included counterions of LJ diameter $\sigma_{\mathrm{ci}} = 0.5\sigma$, but the counterion diameter $\sigma_{\mathrm{ci}} = 1.0\sigma$ was also considered (the latter are discussed further in the Supporting Information). The bead−counterion LJ interaction is additively mixed. Counterions and charged beads have charges of +1e and −1e, respectively, and experience a long-range Coulomb potential as described below. A Langevin thermostat with damping constant of 1.0 and a reduced temperature of $T^* = kT/\varepsilon_{\mathrm{LJ}} = 1.0$ is used in all simulations, where kT is the thermal energy. All beads and counterions have unit mass. The LAMMPS[30] MD program[31] was used to perform the simulations, including its implementation of the particle−particle particle-mesh method to account for long-range electrostatics.[32]

The strength of the Coulombic interaction between two beads with charges q_1 and q_2 is set by the dielectric constant of the medium, ε_r:

$$U_{\mathrm{C}}(r) = \frac{q_1 q_2}{4\pi\varepsilon_0\varepsilon_r r} \quad (3)$$

where ε_0 is the vacuum permittivity. At constant temperature, ε_r is inversely proportional to the Bjerrum length, $l_B = e^2/(4\pi\varepsilon_0\varepsilon_r kT)$, defined as the distance at which the Coulomb interaction equals kT, where e is the elementary charge. In our simulations, the dimensionless quantity σ/l_B was varied from 0.028 to 0.070 in increments of 0.014. To translate e into our LJ unit system or report the ε_r of the medium from the dimensionless σ/l_B requires a choice of σ and temperature in real units. Each uncharged polymer bead maps to approximately three CH_2 units in a polyethylene backbone,[28] so we choose the average bond length of a FENE bond, 0.97σ, to approximate the distance covered by three C−C bonds along the backbone, yielding $\sigma = 0.4$ nm. At room temperature the σ/l_B range used then corresponds to $\varepsilon_r = 4$−10. This ε_r accounts for all parts of the dielectric constant (including the polarizability of all atoms and partial charges which would be on each atom in a fully atomistic model) that are not due to fluctuations in the locations of ions, the part which is included

dx.doi.org/10.1021/ja209142b | J. Am. Chem.Soc. 2012, 134, 574−587

in our model. Without ionic groups, ε_r ranges from ~2 for polyethylene to ~10 for poly(ethylene oxide), but adding polarizable ionic groups and counterions should contribute more to the dielectric constant than is accounted for by the motion of the unpolarizable charges themselves. A priori, we would expect that an ε_r somewhat greater than 2 would best represent an experimental polyethylene-based ionomer, depending on the fraction of groups with larger polarizabilities. As explained in our prior letter,[25] the glass transition of our model system is between $\varepsilon_r = 2$ and 4, and we therefore focus on $\varepsilon_r = 4$ ($l_B/\sigma = 36$), which allows equilibration of the system but also shows strong ionic aggregation. Our mapping of three CH_2 units or 0.4 nm to a polymer bead also suitably corresponds with the size of a COO^- group.[33] The counterion diameter 0.5σ maps well to the ionic diameter of Na^+ of ~0.2 nm. The system packing fraction $\eta_t = (\rho_{ci}\sigma_{ci}^3 + \rho_B\sigma^3)\pi/6$ was set to $0.7\pi/6 = 0.366$, in the range typical of polymer melts, where ρ represents number density and the subscripts ci and b stand for counterions and polymer beads, respectively.

We vary the number of backbone beads per charged bead, N_{bb}. The periodically spaced pendant systems with $N_{bb} = 3$, 5, and 7 resemble the experimental precise PEAA copolymers with 9, 15, and 21 backbone carbons between acetic acid groups, if they were fully neutralized with Na^+. We also study the longer spacings of $N_{bb} = 9$ and 11. The charged beads are placed in the middle of the periodic repeating unit such that charged beads are never on the ends of the chain (analogous to the experimental precise ionomers). For the periodic spacings of $N_{bb} = 3$ and 9, there are a total of 36 backbone beads per chain. In the case of the periodic spacings of $N_{bb} = 5$ and 7, there are 35 backbone beads per chain, while there are 44 backbone beads per chain for the periodic spacing of $N_{bb} = 11$. This yields a molecular weight of ~2 kg/mol after mapping to a PEAA polymer, which is 1−2 orders of magnitude smaller than the experimental molecular weight.[26] We expect that the behaviors of interest here such as ionic aggregate morphology are not affected significantly by molecular weight. Our chain length allows us to equilibrate more easily and stay below the entanglement length. The entanglement length of Kremer−Grest model polymers at a higher density ($\rho\sigma^3 = 0.85$) and with no charges has been reported to either be similar to[28] or longer than[34] our polymers' length, so at our lower density we do not expect any significant entanglement effects.

We approximate fully random linear copolymers by placing charged beads (of various total concentration) randomly along the backbone of the chain such that all backbone beads in the box have the same probability of being charged (for ionenes) or having an attached charged group (for pendants). These fully random ionomers each have 36 backbone beads, though the particular sequences of and total number of charges on each is random. The charged groups can be adjacent to each other and can be at the end of the chain.

Randomness in acid group spacing was also added in a blocky fashion to create materials roughly analogous to experimentally synthesized pseudorandom copolymers. The pseudorandom experimental copolymers were synthesized by ring-opening metathesis in which cyclic monomers with and without a COOH group were copolymerized, yielding COOH groups which were not precisely spaced but which were never placed on the ends of the polymer nor closer than seven backbone carbons apart.[26] Similarly, our random block copolymers are created from blocks of three backbone beads each (which maps to nine backbone C−C bonds). Each block may be uncharged or have a charged bead in the middle (for ionenes) or pendant to the middle bead (for pendants). The charged and uncharged blocks are linked in a random order to create chains of different sequences of 36 backbone beads each; simulations are performed for various average ratios of charged to uncharged blocks. Fully random polymers are created with an average of $N_{bb} = 3$, 5, 7, or 9 backbone beads per charged bead. Random block ionomers are created with $N_{bb} = 5$, 7, or 9 (at $N_{bb} = 3$ this random block model would be composed of only charged blocks and thus would no longer be random). Different types of architectures of the simulated ionomers are shown schematically in Figure 2.

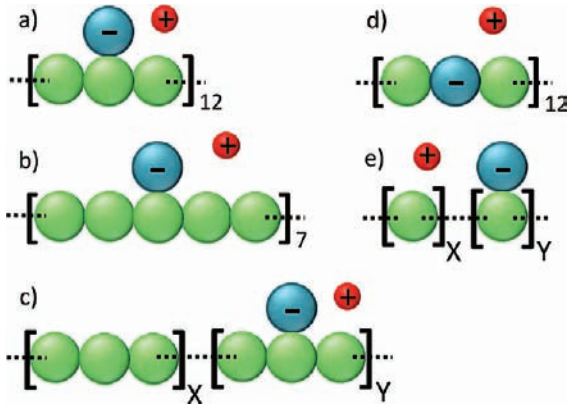

Figure 2. Schematics of simulated polymers with uncharged polymer beads in green, charged polymer beads in blue, and counterions in red: (a) periodic pendants with $N_{bb} = 3$, (b) periodic pendants with $N_{bb} = 5$, (c) random block pendants where the X and Y units are combined randomly and $X + Y = 12$ for each chain ($X/Y = 2/3$, 4/3, and 2 correspond to $N_{bb} = 5$, 7, and 9, respectively), (d) periodic ionenes with $N_{bb} = 3$, and (e) fully random pendants where $X + Y = 36$ for each chain ($X/Y = 2$, 4, 6, and 8 corresponds to $N_{bb} = 3$, 5, 7, and 9, respectively). Polymers a−c here are analogous to fully monovalent-neutralized ionomers based on the acid copolymers of Figure 1a−c.

Unless otherwise noted, the simulation box contained 800 polymers, and polymers and counterions were placed in the box randomly and equilibrated for 10^7 time steps of 0.005τ, where $\tau = (m\sigma^2/\varepsilon_{LJ})^{1/2}$ is the dimensionless time unit. The simulation was then performed for 10^7 time steps or more, during which at least 100 snapshots (equally spaced in time) were saved and analyzed. All reported properties (other than images and the mean squared displacement) are averaged over these snapshots unless otherwise noted.

The mean squared displacement (MSD) of the polymer centers of mass and of the counterions was calculated after subtracting the small total system center of mass displacement. For both ionenes and pendants, fewer ions (larger N_{bb}) leads to slower dynamics. Of all systems discussed here, the smallest MSD during the main data collection period of 10^7 time steps was for the pendant ionomers at $N_{bb} = 11$, $\varepsilon_r = 4$, and $\sigma_{ci} = 0.5$. Its polymer center-of-mass MSD = $8.9\sigma^2$, somewhat less than the polymer mean squared radius of gyration $R_g^2 = 12\sigma^2$ for this system, and its counterion MSD = $38\sigma^2$ by the end of the original simulation time. Most systems moved significantly faster, with the largest MSDs at $\varepsilon_r = 4$ being $120\sigma^2$ for the polymer centers of mass and 1800 σ^2 for counterions, for the case of periodic ionenes at $N_{bb} = 3$. During the prior equilibration period (after a standard soft potential was used to push any overlapping beads off of each other and before data

dx.doi.org/10.1021/ja209142b | J. Am. Chem.Soc. 2012, 134, 574−587

collection), the polymer center-of-mass MSD for all systems was already greater than R_g^2, presumably because the polymers initially moved slightly faster from the random initial configuration toward a more favorable configuration. This suggests that most effects of the initial configuration were erased before data collection began. As another measure of the relaxation from the initial configuration, we calculated the decay of the average polymer end-to-end vector autocorrelation over the equilibration period for the $\varepsilon_r = 4$, $\sigma_{ci} = 0.5$ systems. For all but the slowest system, the average polymer end-to-end vector autocorrelation function (normalized to 1 at time 0) had already decayed to less than 1/e before data collection. For the slowest system (periodic pendants at $N_{bb} = 11$), starting from the initial configuration, this autocorrelation function had not yet reached 1/e by the start of data collection and remained above 1/e for the first quarter of the main data collection period.

Even for the slowest systems, the change in the partial pair correlation functions $g_{ij}(r)$ over the simulation time is negligible on the scale of the figures presented here. Several of the slower systems were simulated further for 2−7 times the initial simulation time, and the change in $g_{ij}(r)$ over this time was extremely small. Note that the simulation time in this broader study is a quarter of that used in our prior work.[25] While little difference in structure is found with longer simulations, the longer time simulation data will be extensively analyzed to better explore the long time dynamics in a future publication.

Here we focus on structural properties of the ionic aggregates and on comparison of the simulation structure factors to experimental data. Partial pair correlation functions were calculated using the visualization software VMD[35] that was also used to create images.[36,37] Partial structure factors $S_{ij}(k) = \delta_{ij} + \rho_i h_{ij}(k)$ were calculated from a Fourier transform of $h_{ij}(r) = g_{ij}(r) - 1$. Clusters, or ionic aggregates, were defined by grouping any oppositely charged ions within a distance of 0.9σ of each other into the same aggregate. The aggregates' centers of mass, principal moments of inertia, size (total number of cations and anions in the aggregate), and spatial extent were recorded, and from the positions of the centers of mass, $g_{CM-CM}(r)$ and $S_{CM-CM}(k)$ were calculated. We include the small number of "clusters" of size 1 in the cluster analysis results except for the moment of inertia calculation. Finally, the polymers' radius of gyration tensors and average R_g^2 were calculated; except for the slightly longer chain $N_{bb} = 11$ polymers, R_g^2 was between 9.5 and $10.7\sigma^2$ for all architectures studied with $\sigma_{ci} = 0.5$.

RESULTS

Real-Space Structure. *Simulated Ionic Aggregate Morphology.* Ionomers of all architectures formed ionic aggregates. Previously, we presented snapshots of a pendant and ionene system to show the discrete aggregates in the pendant case versus the large percolated ionic structure in the ionene case at $N_{bb} = 9$ and $\varepsilon_r = 4$.[25] As a first view at the effect of randomness in spacing on the real space structure of the ionic aggregates, we compare periodic, random block, and fully random ionenes and pendants at $N_{bb} = 9$ and $\varepsilon_r = 4$ in Figure 3. Only the charged beads and counterions are shown, and they are colored by size to delineate the different distinct aggregates. For each of the ionene systems, a percolated aggregate spans the simulation box in three dimensions and is colored transparent yellow. The center of mass of each discrete aggregate is in the periodic box and these aggregates are each drawn contiguously (not broken by the periodic boundary). Visually, the periodic and random ionene systems appear to be relatively similar to each other, and their aggregates are locally thin and stringy. Changing from periodic to random spacing of charged pendant beads instead qualitatively changes the pendant systems' aggregate morphology. The periodic pendant system shows discrete, roughly spherical aggregates with a relatively narrow size distribution. The random block and fully random pendant systems also have discrete aggregates, but with a much wider range of aggregate sizes. The smaller aggregates of the random pendant ionomers are roughly spherical, while the larger aggregates are more extended and resemble short thick strings of a similar width as the more spherical pendant ionomer aggregates. Percolated ionic structures are typically assumed to provide increased conductivity of ions through the sample. Our preliminary calculations show that the counterion diffusion constant is larger for most of our percolated systems than for most of our nonpercolated systems, but we defer a more detailed analysis of the counterion dynamics to a future publication.

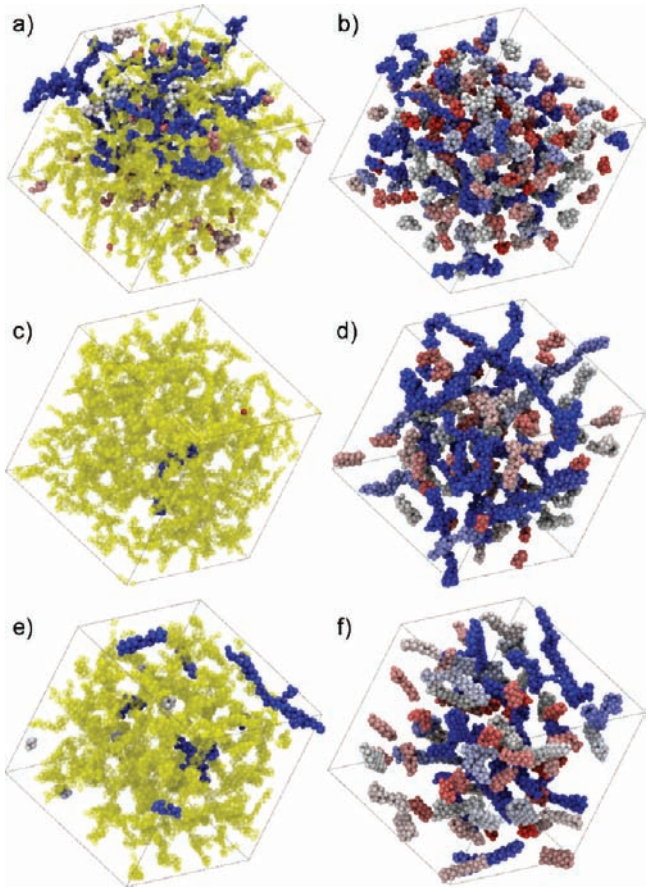

Figure 3. Snapshots of various architectures of ionomers with $N_{bb} = 9$, $\sigma_{ci} = 0.5$, and $\varepsilon_r = 4$: (a) periodically spaced ionenes, (b) periodically spaced pendants, (c) random block spaced ionenes, (d) random block spaced pendants, (e) fully randomly spaced ionenes, and (f) fully randomly spaced pendants. Only counterions (smaller spheres) and charged beads (larger spheres) are shown (uncharged polymer beads are invisible). Based on our cluster analysis results, aggregates are either percolated (shown in transparent yellow) or discrete. Discrete aggregates are colored from red to white to blue in order of increasing number of ions in the aggregate, where the pure red and blue aggregates are more than 1 standard deviation away from the average size for their system.

dx.doi.org/10.1021/ja209142b | J. Am. Chem.Soc. 2012, 134, 574−587

The counterion−counterion structure factors of these systems shown in Figure 3 are given in Figure 4. Interestingly,

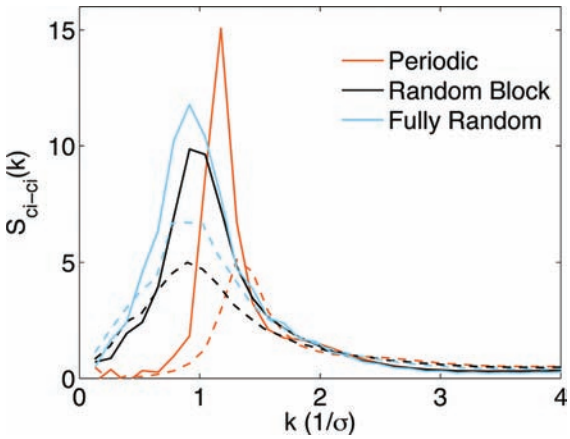

Figure 4. Counterion−counterion structure factors of ionene (dashed lines) and pendant (solid lines) ionomers at N_{bb} = 9 having periodic or random spacings as noted in the legend, with σ_{ci} = 0.5 and ε_r = 4.

the various architectures of ionomers, which show qualitatively different ionic aggregate morphologies, all yield a strong ionomer peak at low wavevector with a small shoulder to the right of the peak. Ionenes have a less intense ionomer peak than pendants, and their peak's shoulder is at a higher wavevector. Changing from a periodic to random spacing of charged beads broadens the ionomer peak and shifts it to lower wavevectors. (These statements are for N_{bb} = 9; see further discussion of the ionomer peak height and location below.)

The cluster analysis results for all ε_r = 4, σ_{ci} = 0.5 systems are summarized in Figures 5 and 6. Figure 5 shows the fraction of ions involved in aggregates which span the box in at least one dimension, f_{span}. For all systems at N_{bb} = 3, due to the large total concentration of ions, nearly all ions are in a large percolated structure which crosses the box in all three dimensions. As the ion concentration is lowered by increasing N_{bb}, fewer ions are in box-spanning aggregates, and some of the spanning aggregates cross the box in only one or two dimensions. For periodic ionenes at N_{bb} = 11, an aggregate percolates through the box in 3D in less than half of the snapshots. For periodic and random pendants at N_{bb} = 9 or larger, hardly any aggregates span the box. Overall, aggregates in ionene systems more easily percolate than those of pendants, and aggregates in the random types of ionomers percolate more easily than in periodic ionomers. Figure 6 gives the average size of aggregates (in number of ions per aggregate) which do not span the simulation box. At low N_{bb} or for most ionenes, these discrete aggregates are small and relatively rare, though they become more common and larger with increasing N_{bb}. For periodic pendants at N_{bb} = 7, 9, and 11, no ionic structures span the box and the aggregates' average size slightly decreases with N_{bb}. For these systems only, there is a relatively narrow size distribution of aggregates and the standard deviation in aggregate size is significantly smaller than the average aggregate size (a table of the standard deviation in n_{agg} is included in the Supporting Information). Both random block and fully random pendants at N_{bb} = 9 rarely have an aggregated structure larger than the box. However, the random pendants' discrete aggregates are much larger than those of the periodic pendants, as seen in Figure 3.

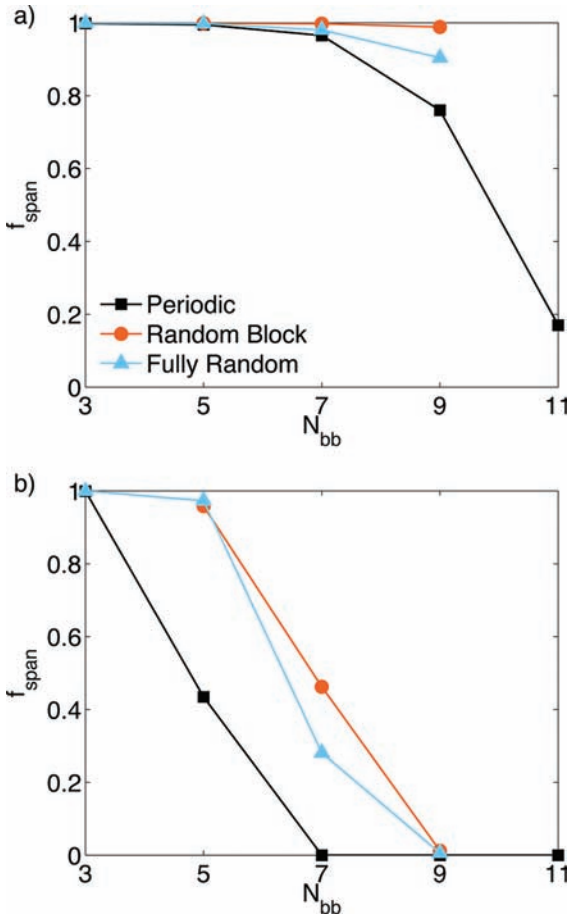

Figure 5. Fraction of ions in aggregated structures which span the simulation box for (a) ionene and (b) pendant ionomers as a function of spacing at σ_{ci} = 0.5 and ε_r = 4. The charged bead spacing is periodic (square data points), random block (circles), or fully random (triangles).

To quantify the shape of the aggregates, we calculated their average shape anisotropy $\langle\kappa^2\rangle$. Many different metrics can be calculated to quantify average polymer or cluster shape.[13,38−41] We use $\langle\kappa^2\rangle$ which varies simply from 0 for spheres to 1 for straight rods. $\langle\kappa^2\rangle$ can be calculated from the eigenvalues of the radius of gyration tensor or from the (closely related if all polymer or cluster units have equivalent mass) eigenvalues of the moment of inertia tensor, λ_1, λ_2, and λ_3, also known as the principal moments of inertia, using eq 4.[38,39]

$$\kappa^2 = 4 - 12\frac{\lambda_1\lambda_2 + \lambda_1\lambda_3 + \lambda_2\lambda_3}{(\lambda_1 + \lambda_2 + \lambda_3)^2} \quad (4)$$

The average aggregate shape anisotropy (excluding box-spanning aggregates and singlets) is lower for the periodic pendant systems at N_{bb} = 7, 9, and 11 than for all other architectures at ε_r = 4 and σ_{ci} = 0.5. The systems where extremely few of the aggregates span the box (such that almost all ions are included in the measure of average shape anisotropy) are periodic pendants at N_{bb} = 7, 9, and 11 ($\langle\kappa^2\rangle$ = 0.34, 0.26, and 0.23, respectively), random block pendants at N_{bb} = 9 ($\langle\kappa^2\rangle$ = 0.43), and fully random pendants at N_{bb} = 9 ($\langle\kappa^2\rangle$ = 0.49). For periodic ionenes at N_{bb} = 11, only 18% of ions participate in box-spanning aggregates, and for other nonsinglet aggregates, $\langle\kappa^2\rangle$ = 0.46. At the increased ε_r = 6, there were no box-spanning aggregates in our simulations of periodic

dx.doi.org/10.1021/ja209142b | J. Am. Chem.Soc. 2012, 134, 574−587

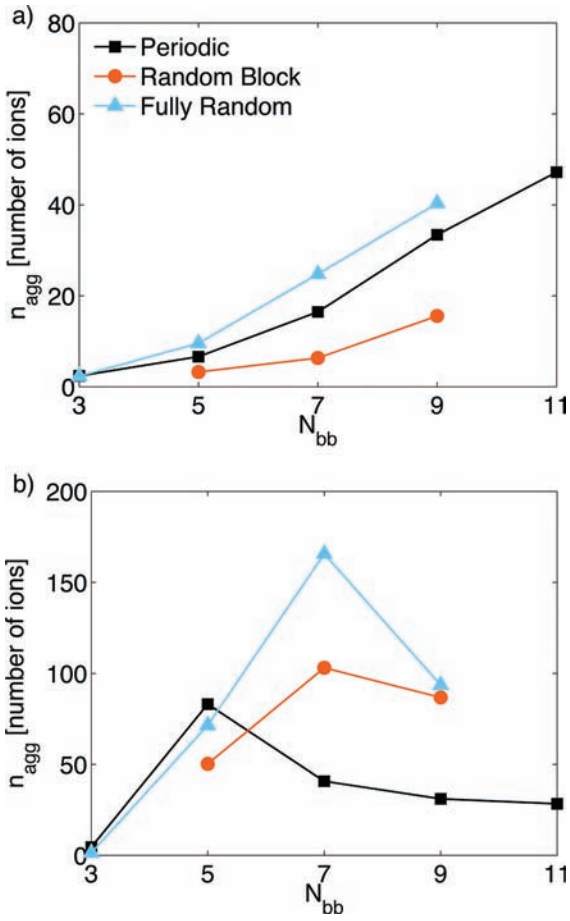

Figure 6. Average aggregate size (number of ions per aggregate) for aggregates which do not span the simulation box for (a) ionene and (b) pendant ionomers as a function of spacing at $\sigma_{ci} = 0.5$ and $\varepsilon_r = 4$. The charged bead spacing is periodic (square data points), random block (circles), or fully random (triangles).

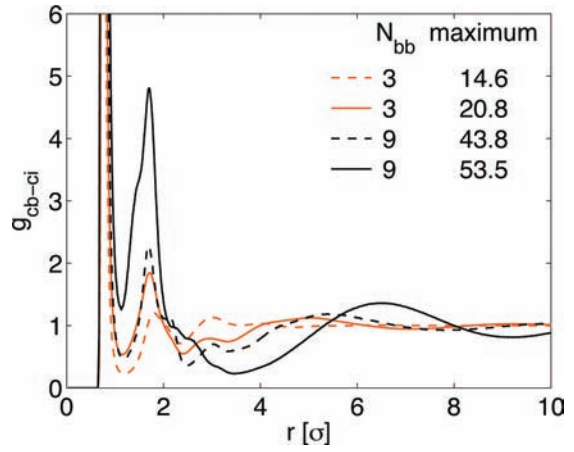

Figure 7. Charged bead−counterion partial pair correlation functions for periodic ionene (dashed lines) and pendant (solid lines) ionomers at $N_{bb} = 3$ and 9, $\sigma_{ci} = 0.5$, and $\varepsilon_r = 4$. The global maximum of each function is noted in the legend.

ionenes and pendants,[25] and $\langle\kappa^2\rangle$ is lower for pendants (0.45) than for ionenes (0.57). The Supporting Information gives $\langle\kappa^2\rangle$ for all systems. As observed in the snapshots presented above, these values of $\langle\kappa^2\rangle$ show unambiguously that the periodic pendant architecture yields more spherical aggregates than random pendants and periodic ionenes.

Pair Correlation Functions. The ion−ion partial pair correlation functions reveal the averaged ion structure in real space. In Figures 7 and 8, we present results for ionenes and pendants at a short and long spacing of charged beads to show the effects of the pendant architecture and spacing. The charged bead−counterion correlation function (Figure 7) has a sharp peak around 0.75σ, the distance of charged bead−counterion contact (at which the LJ repulsion ends). Other short-range peaks depend on the ionomer type. All g_{cb-ci} except that of ionenes with a short spacing have a broad, long-range peak between ~4 and 7σ. As we discussed in our prior work[25] and further explain below, this peak corresponds to the mesoscale order which exists either within large percolated aggregates or between distinct aggregates. Both the short- and long-range order is stronger at longer spacings (lower ion content) and stronger for pendants than for ionenes.

Similar trends are found for the counterion−counterion pair correlations in Figure 8a for periodic ionene and pendant ionomers. In this case, the first and second peaks are at $1.1\sigma \approx \sqrt{2}(0.75\sigma)$ and $1.4-1.5\sigma \approx 2(0.75\sigma)$, which corresponds to the distances between like charges in a flat quadrupole of ions and in a linear chain of four ions, respectively. The second peak is relatively more prevalent for ionenes than for pendants, suggesting that ionenes' aggregate structures may be more extended locally while pendants may form more compact structures. For $N_{bb} = 3$, beyond these first peaks are further small oscillations at $\sigma \approx 2-4$ in approximately opposite locations in g_{cb-ci} and g_{ci-ci}. Similar but more prevalent oscillations were observed in prior simulations of a model similar to our ionenes at $N_{bb} = 2$, and simply correspond to molten NaCl-like charge ordering.[24] They are less prevalent at higher N_{bb}. The long-range peak of Figure 8a is similar to that in the charged bead−counterion correlations in Figure 7.

Parts b and c of Figure 8 are analogous to Figure 8a for the random block and fully random models, respectively. The local ordering peaks generally become more intense going from periodic to random block to fully random spacing. Adding randomness in either fashion greatly decreases the long-range peak in $g_{ci-ci}(r)$. For random pendants at both short and long spacing, the long-range peak is still visible but is moved to even larger r. The snapshots of Figure 3 visually show the relative similarity in the local order and significant variation in long-range order of the $N_{bb} = 9$ ionomers of different architectures.

Scattering and Structure Factors. *Experimental Comparison.* Due to the difficulty of directly measuring the real space structure, the averaged ionic aggregate structure is typically probed by scattering experiments. The low wavevector scattering peak is a measure of the size and mesoscale order of ionic aggregates. Our coarse-grained model is meant to capture the basic results of strong ionic interactions in the presence of the constraints imposed by the polymer backbone, and shows a strong ionomer peak.[25] To further confirm the experimental relevance of our model, we compare the experimental X-ray scattering to simulation results. As discussed above, the precise and pseudorandom PEAA copolymers neutralized with Na^+ correspond to our simulated pendant ionomers at $\sigma_{ci} = 0.5$, where one bead represents three C−C bonds. The experimental materials were partially neutralized with Na^+ but still contained many COOH groups which are potentially dimerized with each other or involved in aggregates. However, we do not attempt to consider the detailed local chemistry with

dx.doi.org/10.1021/ja209142b | J. Am. Chem.Soc. 2012, 134, 574−587

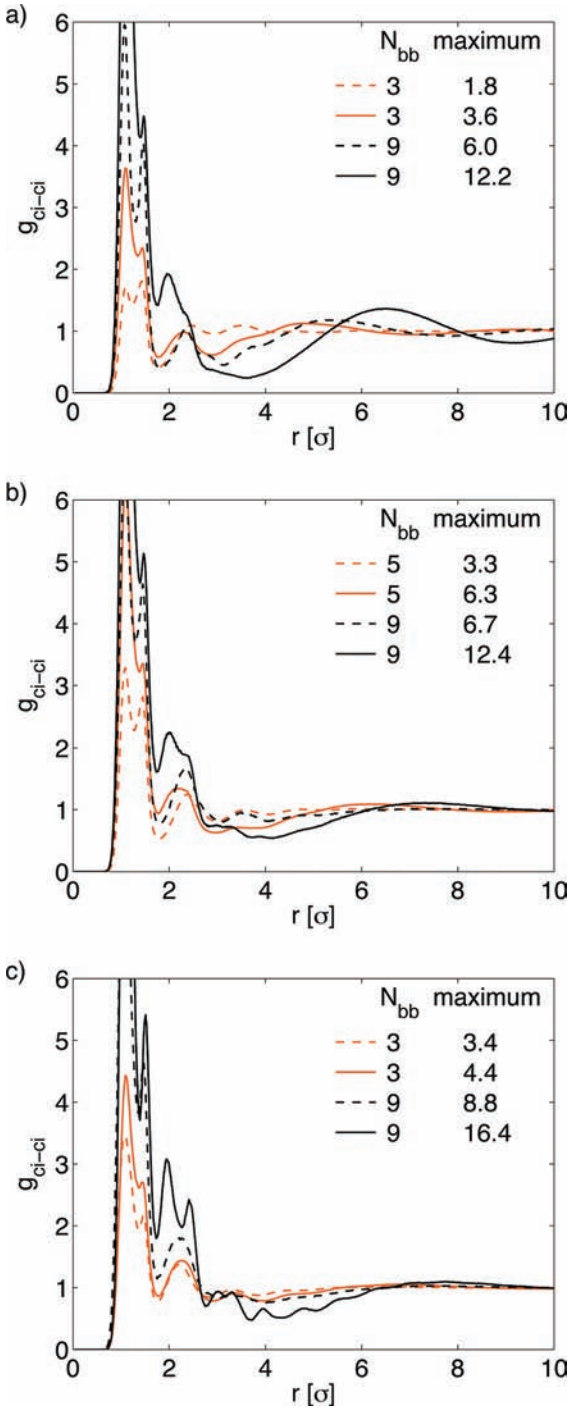

Figure 8. Counterion−counterion partial pair correlation functions for ionene (dashed lines) and pendant (solid lines) ionomers with σ_{ci} = 0.5, and ε_r = 4 and (a) periodic spacings N_{bb} = 3 and 9, (b) random block spacings N_{bb} = 5 and 9, and (c) fully random spacings N_{bb} = 3 and 9. The global maximum of each function is noted in the legend.

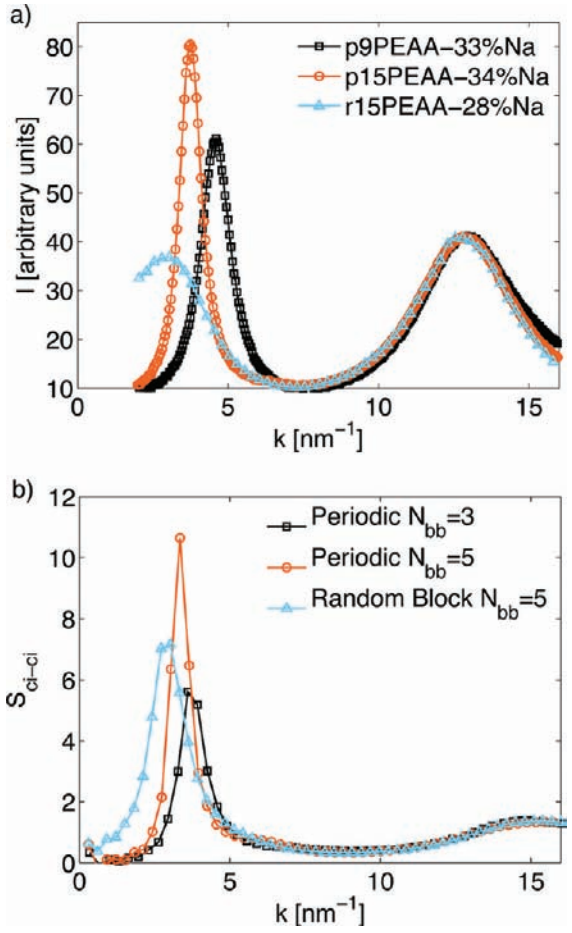

Figure 9. (a) Experimental scattering data for p9AA-33%Na (squares), p15AA-34%Na (circles), and r15AA-28%Na (triangles). (b) Simulation counterion−counterion partial structure factors for fully neutralized pendant ionomers of analogous architectures to (a), with σ_{ci} = 0.5 and ε_r = 4. The charged bead spacing is periodic with N_{bb} = 3 (squares) or N_{bb} = 5 (circles), or random block with N_{bb} = 5 (triangles).

our coarse-grained polymer model. Instead we simulate only fully neutralized ionomers. Related experiments on precise Zn^{2+}-neutralized PEAA ionomers showed relatively little change in ionomer peak location with increasing neutralization.[4]

The experimental curves in Figure 9a present the total scattering of all atoms of the PEAA copolymers, partially neutralized with Na^+, as drawn in Figure 1. The low wavevector ionomer peak is attributed to scattering between the aggregates which have an increased electron density from Na^+ and from the oxygens in the COO^- groups. The higher wavevector amorphous halo arises from the local liquid-like packing of the polymer. The relative heights of the ionomer peaks are not exact, since the experimental data are not in absolute intensity units. Instead, all curves have been matched in intensity at a point in the amorphous halo and at a point in the trough before the halo, so if these polymer architectures have significant differences in their amorphous halos, then the relative heights of their ionomer peaks as shown here would not be reliable. We expect that the amorphous halos, set by the polyethylene backbone, are likely similar for these materials, but we do not base our conclusions on the relative heights of the experimental ionomer peak. We note that polyethylene crystallites are expected in these types of materials at low temperatures, but to avoid this complication the materials were held at 118 °C during the X-ray scattering, and scattering features of crystallites are not present.

From the simulation we calculate the partial structure factors, which can be weighted by the scattering lengths of the atoms that each bead represents and added together to obtain an estimate of the total scattering. Because our mapping of beads to atoms is approximate and all ion−ion partial structure factors

dx.doi.org/10.1021/ja209142b | J. Am. Chem.Soc. 2012, 134, 574−587

have a similar ionomer peak (the location and shape of the ionomer peak is similar for the total or individual structure factors), we simply present the counterion−counterion structure factors in Figure 9 b, converted to nm^{-1} using σ = 0.4 nm, for the systems analogous to the experimental ionomers as shown in Figure 2. Because the polymer backbone scattering is not included, the amorphous halo of experiments and the counterion−counterion local ordering peak of the simulations should not be compared, and we note that even the backbone bead−backbone bead structure factor of a coarse-grained model would not be expected to precisely match that of an atomistic or experimental system.

Figure 9 shows that the major experimental trends of the ionomer scattering peak match the simulations. Our physically motivated mapping of the bead size to nanometers places the simulated ionomer peak in approximately the same place as the experimental peak. For precise materials, increasing the spacing between ions along the chain moves the peak to lower wavevector. In other words, a longer spacing leads to a longer length scale of real-space order. Experiments and simulations also show the same effect of randomness at constant mean spacing. Moving from the experimental precise to pseudorandom materials or from the simulation periodic to random block models broadens the ionomer peak and moves it to a lower wavevector.

Ionomer Peak Trends. Figures 10 and 11 show the ionomer peak height and its wavevector location, respectively, for all ε_r = 4, σ_{ci} = 0.5 systems. $S_{ci-ci}(k)$ is composed of discretely spaced points, the largest of which is considered to be the peak height. This gives an error of several percent for the sharper peaks depending on whether the peak location coincides closely with a discrete point; however, a more complex analysis of the shape of the peak and its exact maximum was not necessary to discuss the trends of interest here. The most intense ionomer peaks are for systems with roughly spherical aggregates: the periodic pendants at N_{bb} = 7, 9, and 11. Even the other pendant systems with large stringy or percolated aggregates have more intense peaks than the analogous ionenes. At constant average spacing, adding blocky randomness decreases the peak height for pendants but does not appreciably change the ionene peak height. Interestingly, when the ions are percolated (ionenes and low N_{bb} pendants), changing from a periodic to fully random spacing increases the ionomer peak height, while the opposite is true for systems with discrete aggregates (high N_{bb} pendants). The peak locations (Figure 11) of both ionene and pendant random materials are relatively similar to each other and lower than those of periodic systems, suggesting that adding randomness in the molecular architecture increases the length scale of mesoscale order. The precise ionenes at low N_{bb} have the highest peak location or shortest length scale of real space order, and their ionomer peak moves to lower wavevectors with increasing N_{bb}. The pendant peak also moves to lower wavevector with increasing N_{bb}, although to a lesser extent.

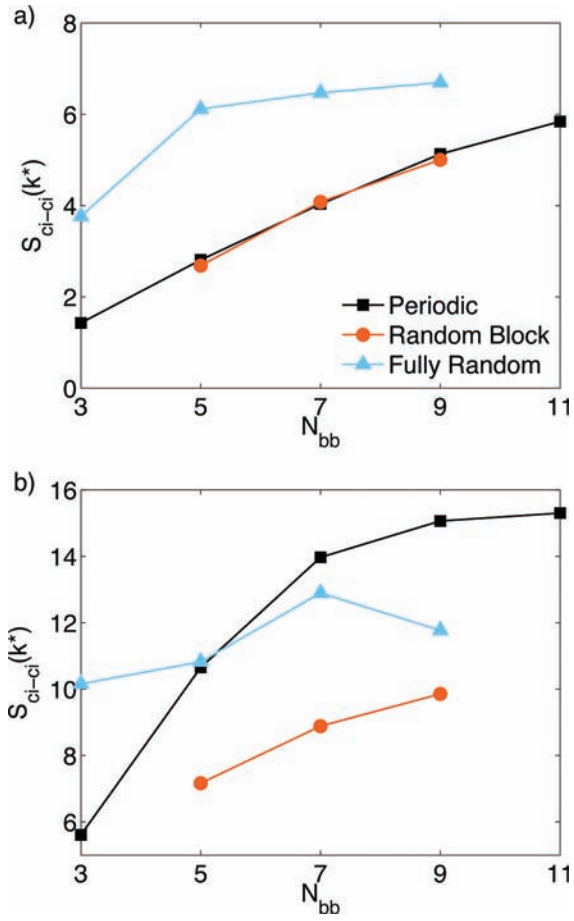

Figure 10. Height of the ionomer peak in S_{ci-ci} for (a) ionene and (b) pendant ionomers as a function of spacing at σ_{ci} = 0.5 and ε_r = 4. The charged bead spacing is periodic (square data points), random block (circles), or fully random (triangles).

DISCUSSION

Shape and Size of Aggregates. In the simulations we observe dense ionic aggregates that are relatively small and roughly spherical for some systems and are large (sometimes percolated through the box), more extended, and stringlike for others. A general rule across all systems is that very large aggregates are extended rather than spherical. Consider a perfect cube of ions that is three ions wide in an NaCl arrangement with a counterion in the center. Such a structure could form for the pendant systems with each charged bead on the outside of the crystal such that the backbone to which it is bonded is outside of the crystal. Although more ions could be added to some of the facets, the crystal cannot grow another complete layer in all directions because of the neutral backbone beads occupying sites in the lattice. For the case of ionenes, making even a three ion wide crystal requires a sharp bend in the backbone near at least six charged beads on the faces, which is possible in our freely jointed model but will have an entropic cost. This may explain why ionenes are less likely to form roughly spherical aggregates than pendants and instead form thinner stringy structures. Considering dense ion-only aggregates as found in our simulations, if the aggregates are significantly larger than about 3^3 = 27 ions, they must extend in one or two dimensions and be one or two ions wide in the third dimension (although this disklike or stringlike structure could be bent or branched). Note that this is simply a geometric argument; in our simulations the ions are not exactly in an NaCl arrangement. Even aggregates of size 27 (which are unusual because most aggregates are charge neutral) or 28 are rarely observed in near-perfect cubelike 3 × 3 × 3 configurations. For the most closely spherical aggregate system (lowest $\langle\kappa^2\rangle$), precise pendants at N_{bb} = 11, the average aggregate size is 28 ions. The largest aggregates in this and the other roughly spherical aggregate systems do appear more stringlike, as seen in Figure 3b. Interestingly, when comparing

dx.doi.org/10.1021/ja209142b | J. Am. Chem.Soc. 2012, 134, 574−587

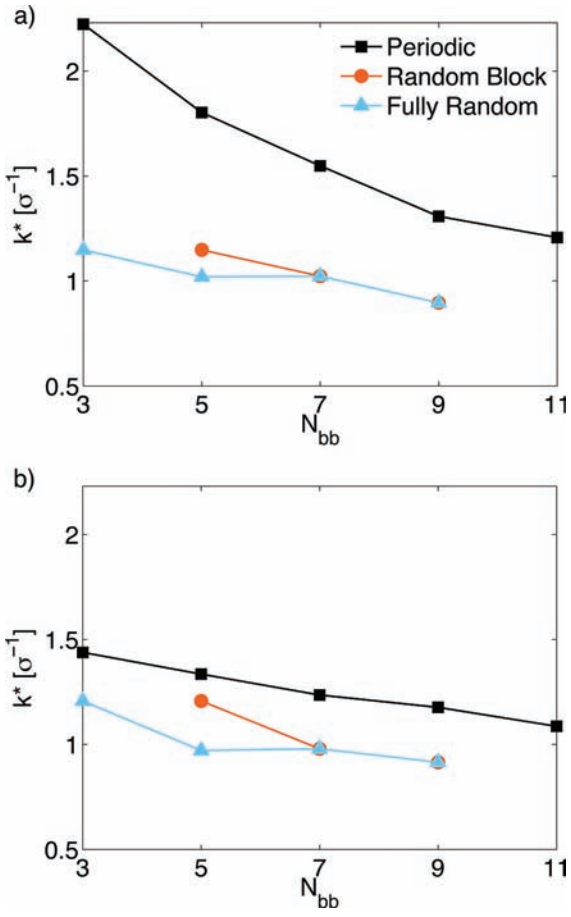

Figure 11. Location, k^*, of the ionomer peak in $S_{ci-ci}(k)$ for (a) ionene and (b) pendant ionomers as a function of spacing at $\sigma_{ci} = 0.5$ and $\varepsilon_r = 4$. The charged bead spacing is periodic (square data points), random block (circles), or fully random (triangles). Depending on the system, the $S(k)$ was calculated with a discrete spacing in k space of ~0.12–0.13σ^{-1}; thus, this is the resolution of the data points shown here.

aggregates of the same size, they are relatively similar across all architectures of pendants or across all architectures of ionenes. Ionenes and pendants differ in that the ionene aggregates become more extended or less spherical at smaller aggregate sizes; the snapshots in Figure 3 and in our prior work[25] show that extended pendant aggregates often have a cross section of about four ions, while ionenes' aggregates more often have a cross section of two ions. Comparing $\langle\kappa^2\rangle$ of aggregates of exactly size 28 across several different architectures shows that aggregates of this size are relatively more spherical for various types of pendants than for ionenes (values are tablulated in the Supporting Information).

Simulations of at least two related systems have also shown spherical or globular clusters. Ayyagari et al. simulated polymers with two sticky groups each either within or at the ends of the chain, and both architectures formed roughly spherical clusters.[13] The former architecture would be similar to a short version of our $N_{bb} = 7$ ionenes if the associating groups had been charged beads instead of stickers (and if counterions were included). The average cluster size for these systems was 13 stickers. Although our most closely related systems (periodic ionenes at $N_{bb} = 7$) were percolated, this number is not too far from the average of ~20 charged beads (~40 ions total) per cluster for the spherical aggregate forming $N_{bb} = 7$ periodic pendants. Allahyarov et al. considered dry Nafion-like ionomers with permanently bound hydrogens rather than free counterions.[22] The acidic groups interacted through a dipole–dipole attraction, an additional Yukawa-type attraction, or both. Some systems showed a peak in the structure factor apparently corresponding to the ionomer peak, and the added attraction could cause dense globular clusters to form, although average cluster sizes were not discussed.

Recognizing that spherical clusters cannot grow large in 3D if composed of short ionic segments, some authors have suggested that a cluster may be a (uncharged polymer filled) spherical shell, a core surrounded by polymer, and then a spherical shell, or a flat disk.[1,14] The shell configurations do not seem likely in a system such as ours and were not observed. Considering dense ion packing as observed in our systems, the shell would have to be one or two ions thick. If it were two ions thick, the curvature of the shell would distort the packing of ions in different layers. Trapping polymer backbone segments inside of a spherical shell could also have a high entropic cost, depending on the length of the segments and size of the cluster. In our pendant systems, a polymer would not be able to cross through the shell without placing an uncharged bead in the shell, though ionenes would be able to cross a shell of one ion thick. Furthermore, calculations of only the electrostatic energy of dipoles arranged on the surface of a sphere or in a four dipole cross section cylinder suggest that a cylinder is slightly more favorable for large cluster sizes.[42]

Disk-shaped aggregates seem relatively plausible for our system. The free energy analysis of Semenov et al. suggested that disk-shaped clusters would be preferred over spheres or cylinders.[14] In that case ionomers were analyzed as multiblock copolymers with short strongly attracting blocks. Local monomer-scale packing and long-range electrostatics, which are relevant in our simulations, were not considered. Interestingly, disklike aggregates were observed in coarse-grained simulations of telechelic ionomers of 64 backbone beads each that were otherwise similar to our coarse-grained model.[23] The segments between charged beads in our polymers are significantly shorter, and our polymers have relatively few (or no) ions on the ends of the chains. Thus, as noted above, in order for our polymers to place a charged bead inside a flat surface, a sharp bend in the backbone is required. Apparently either this entropic consideration or the shorter segment lengths considered here prevent large disklike aggregates from forming in our simulations. Earlier simulations using a model similar to our ionenes at $N_{bb} = 6$ showed a somewhat extended and branched (rather than spherical or disklike) and apparently percolated aggregate, as is seen in our ionene simulations.[24]

Aggregate size, the height of the first peak in $g_{ci-ci}(r)$, and the ionomer peak height (to some extent) can be thought of as measures of the general strength of ionic aggregation. In those systems with few box-spanning aggregates (pendants at high enough N_{bb}), a fair comparison of average aggregate size can be made (nearly all ions are in structures included in the aggregate size data, and a single aggregated structure does not dominate). The three periodic pendant systems at $N_{bb} = 7$, 9, and 11 have somewhat decreasing average aggregate sizes of 41, 31, and 28, respectively. The average aggregate sizes of the $N_{bb} = 9$ random block pendants and fully random pendants are much larger at 87 and 93, respectively. A free energy analysis by Nyrkova et al. of associating polymers which assumed spherical clusters suggested that the cluster size grows as the number of associating groups per ionic block cubed (where an ionic block is composed of one or more adjacent associating units). The

dx.doi.org/10.1021/ja209142b | J. Am. Chem.Soc. 2012, 134, 574–587

authors noted that due to this strong dependence, if even a small number of charged groups are adjacent to each other in a random ionomer, its cluster size will increase.[15] The underlying basis for this prediction that applies to our system is that there is a free energy cost for each polymer segment sticking out of an aggregate. In the case of two charged beads adjacent to each other or a charged bead on the end of the polymer, only one polymer segment per bead must incur the entropic cost of stretching away from the aggregate, and the polymer backbone may not have to bend as sharply. In the case of our fully random ionomers at N_{bb} = 9, 25% of all ions are either adjacent to another ion or at the end of the chain. This may lead to a slightly stronger clustering ability of fully random pendants and explain why fully random pendants' aggregates are slightly larger than those of random block pendants. However, random block pendants have no charged beads adjacent to each other or on the ends of the chain, so this argument does not explain why both types of random pendants' aggregates are much larger than those of periodic pendants. We surmise that the periodicity along the chain predisposes the periodic pendants to their special smaller, roughly spherical aggregate morphology, and further discuss increased interaggregate bridging in these systems in the next section. At low N_{bb}, this special periodicity effect may become less important, and the ionomer peak height drops significantly with N_{bb} for periodic pendants. The effect of charged beads adjacent to each other and at the end of the chain increases at low N_{bb}; by N_{bb} = 3, 58% of fully random charged beads are in one of these categories. Interestingly, the fully random pendants have a significantly larger ionomer peak than any random block pendants or than periodic pendants at N_{bb} = 3. Fully random ionenes also have a larger ionomer peak than either periodic or random block ionenes, which are similar to each other. Fully random pendants and ionenes also always have a larger first peak in g_{ci-ci} than their random block or periodic systems at the same N_{bb} (not shown for all systems). This may reflect their adjacent charged beads and polymer-terminating charged beads which are able to aggregate more strongly.

Interaggregate Order and Kinning–Thomas Model. Although all of our simulated systems have some degree of long-range order leading to an ionomer peak in the structure factor, this ordering is strongest for pendant ionomers at high N_{bb}. We previously proposed that in the N_{bb} = 9 pendant case, the long-range peak in $g(r)$ or the ionomer peak in $S(k)$ is primarily due to interaggregate order set by bridging of backbone segments between charged beads.[25] The primary peak in the aggregates' center of mass structure factor (discussed further below) was shown to correspond with the ionomer peak. With decreasing N_{bb}, the pendant ionomer peak moves to higher wavevector, consistent with the idea that the spacing between charged beads helps to set the interaggregate (or in percolated cases, mesoscale intraaggregate) ordering length scale.

Further supporting this idea, adding randomness to the charged bead spacing interrupts the interaggregate ordering: both types of random systems show significantly less long-range order in $g(r)$ and a broadening of the ionomer peak in $S(k)$ versus their periodic analogues. To quantify the degree of interaggregate polymer bridging, we calculated the fraction of segments between charged beads which connected two different discrete aggregates. At N_{bb} = 9 where few of the pendants' aggregates span the box, 76% of periodic pendants' segments are bridges, versus just 38% for random block pendants and 36% for fully random pendants. This increase in bridges for periodic pendants is not simply because their aggregates are smaller. Even for periodic pendants at N_{bb} = 5 where there is typically a large percolated aggregate and the non-box-spanning aggregates have a similar size to that of the random block pendant system, 50% of segments bridge between different aggregates (including box-spanning aggregates). In general, we expect increased bridging would improve the mechanical properties such as the bulk modulus (though an analysis of such properties is beyond the scope of this paper). Overall, for pendant ionomers, the periodic architecture increases bridging between aggregates and has increased interaggregate order versus either random architecture. Note that for periodic systems, segments looping closely back within an aggregate and polymer end segments can also help to set the same approximate length scale of closest approach between aggregates.

The experimental ionomer peak of these and related materials can be fit well with the KT model, a refinement of the YC model.[2,4,5] These models propose that spherical aggregates of radius R_1 and number density ρ_{agg} with constant interior electron density (ρ_1) exist in a lower constant electron density (ρ_0) medium. Further, these aggregates have liquid-like order like hard spheres, with a radius of closest approach R_{CA} that is larger than R_1.[2,5] The overall scattering depends on both the form factor scattering of the spherical aggregates and the interaggregate structure factor. The total scattering $I(k)$ normalized by the scattering of an electron $I_e(k)$ and the volume of material participating in scattering V_s is given by

$$\frac{I(k)}{I_e(k)V_s} = \rho_{agg}(\rho_1 - \rho_0)^2\left(\frac{4}{3}\pi R_1^3\right)^2(\Phi(kR_1))^2 S_{HS}(\rho_{agg}, R_{CA}, k) \quad (5)$$

S_{HS} is the hard-sphere structure factor and $(\Phi(kR_1))^2$ is the form factor of a homogeneous sphere, where

$$\Phi(x) = 3\frac{\sin(x) - x\cos(x)}{x^3} \quad (6)$$

The terms on the right-hand side of eq 5 that do not depend on k can be combined into a single prefactor to set the overall scattering intensity, resulting in a total of four variable parameters. The difference between the YC and KT models is in the specific form of $S_{HS}(k)$; we use the KT model which calculates $S_{HS}(k)$ from the Percus–Yevick equation.[5] While it is straightforward to include the effects of polydispersity in both Φ and S_{HS}, this requires additional parameters and is not discussed here.[5] Depending on the three parameters which affect the shape of the scattering profile, ρ_{agg}, R_1, and R_{CA}, the KT model can yield a sharp peak with a small shoulder to the right of the peak. The shoulder is clearest in our precise, larger N_{bb} systems (the shoulder can be seen in Figure 4 and in the precise N_{bb} = 5 curve of Figure 9b at ~6 nm^{-1}). The KT model can fit many peaks of the same general shape well, including our ionene systems at ε_r = 4. However, at large ε_r = 10 there are small, weak aggregates of a few ions each and many lone single ions, and in that case the KT model does not fit the very weak ionomer peak well (not shown). At ε_r = 4, with most of the ionene's ions in a large percolated structure, the physical meaning of the parameters of the KT model becomes unclear. Without 3D real-space data of ionic aggregates, it has previously been an open question how well the KT model represents ionic

aggregate morphology, even for those systems with discrete aggregates, and several other competing models of ionic aggregate morphology are in use.[1]

Figure 12 shows (a) the counterion−counterion structure factor and (b) the aggregates' center-of-mass to center-of-mass

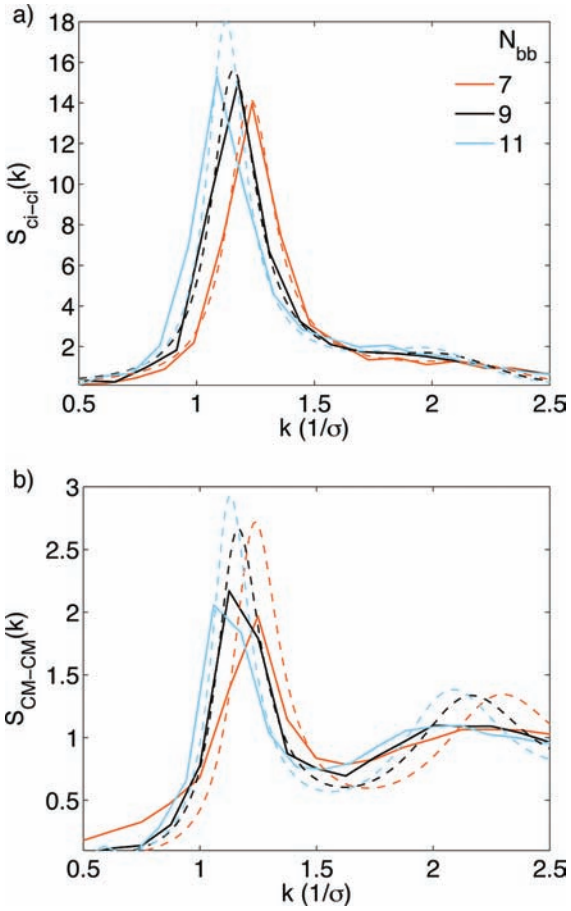

Figure 12. (a) Counterion−counterion structure factors (solid lines) and the KT model fit (dashed lines, least-squares fit to data in the range of $0.5-2.5\sigma^{-1}$) for periodic pendant ionomers with spacings N_{bb} = 7, 9, and 11 at σ_{ci} = 0.5 and ε_r = 4. Data points below $0.5\sigma^{-1}$ are noisy and not shown. (b) Aggregates' center-of-mass to center-of-mass structure factors (solid lines) and the hard-sphere structure factor implemented in the KT fit (dashed lines).

structure factor only for those systems with roughly spherical aggregates of controlled size: the pendant ionomers of periodic spacings N_{bb} = 7, 9, and 11. Both the ionomer peak and the primary aggregate center-of-mass peak decrease in wavevector with increasing spacing, but the peak heights and shapes are similar for these three spacings. The best fit of the four-parameter KT model to $S_{ci-ci}(k)$ is also shown, along with the hard-sphere structure factor used in the model fit. Fitting the periodic pendant N_{bb} = 9 system $S_{ci-ci}(k)$ curve, we find the KT parameters ρ_{agg} = 0.0043 aggregates/σ^3 and $R_1 = 1.4\sigma$. These values are similar to that simulated system's aggregate number density and core size (0.0045 aggregates/σ^3 and 1.5σ, estimated as half the average span of an aggregate in x, y, or z) found from the cluster analysis. Furthermore, the structure factor from the model based on ρ_{agg} and R_{CA} (2.9σ) is similar to the actual aggregate S_{CM-CM} calculated directly from the simulations. The total volume of aggregates calculated from these fitted values of ρ_{agg} and R_1 ($2500\sigma^3$ per simulation box) is similar to the total volume that the ions in the simulation box would fill if they were arranged in an NaCl-type crystal ($2700\sigma^3$, using an ion closest approach distance of 0.75σ). For periodic pendants at N_{bb} = 11, the KT fit also produces a ρ_{agg}, R_1, and aggregate core volume within 10% of those found from direct cluster analysis, and the KT hard-sphere structure factor is similar to S_{CM-CM}.

The comparison between stoichiometric ionic volume (calculated as though the ions were in a crystal) and the KT predicted aggregate core volume is sometimes made experimentally. If the KT model aggregate core volume is smaller than the stoichiometric ionic volume, this suggests that not all ions are contained within the aggregates, while if the opposite is true, one would suspect the aggregates do not consist solely of ions.[2,3] Either case has important implications for the transport and mechanical properties of these materials. In all of our simulated fully neutralized systems at relatively low dielectric, we observe aggregates of approximately crystalline inner density (without intervening polymer backbone). There are also extremely few individual ions, or singlets; for any of the ε_r = 4, σ_{ci} = 0.5 systems, only 0.003−0.02% of ions are not within 0.9σ of another ion. Given that the vast majority of ions are in dense many-ion aggregates, it makes sense that the KT model volume equals our total ionic volume for our systems which aggregate as proposed in the KT model.

For periodic pendants at N_{bb} = 7, the aggregates are not as uniform as they are at N_{bb} = 9 and 11. The KT model fits $S_{ci-ci}(k)$ at N_{bb} = 7 just as well as it does at higher N_{bb} (the mean squared error is similar). However, the N_{bb} = 7 system's KT parameters ρ_{agg} and R_1 differ from its cluster analysis results by 20−25%, and the KT predicted aggregate core volume is 13% lower than the stoichiometric ionic volume (the volume of the known number of ions if they were in a crystal). Hypothetically, an experimental analysis of scattering that matches the N_{bb} = 7 system's $S_{ci-ci}(k)$ may conclude that some ions are dispersed in the uncharged polymer medium instead of being contained within the aggregates. Instead, nearly all of this system's ions appear to be in densely packed aggregates, but the aggregates are not exactly spherical and are somewhat variable in size. In summary, for our discrete, roughly spherical aggregate systems, the parameters ρ_{agg}, R_1, and R_{CA} obtained from a KT model fit do represent approximately the actual aggregate number density, core size, and interaggregate length scale of ordering. Therefore, for experimental systems with spherical aggregates, we expect that parameters obtained from a KT fit of $S(k)$ are accurate measures of the aggregate morphology.

■ CONCLUSIONS

We performed MD simulations on various periodic and random architectures of coarse-grained ionomers including explicit counterions. We also presented X-ray scattering data for precisely spaced and pseudorandom PEAA copolymers that were partially neutralized with Na^+. Experimentally, increasing the spacing of ionic groups along the chain moved the ionomer peak to lower wavevector and adding randomness in the spacing broadened the peak and moved it to lower wavevector. These major trends were also reproduced in the counterion scattering calculated from the simulations.

Both random and periodic ionenes at all charged bead spacings considered formed large ionic aggregates that percolated through the simulation box, although a smaller percentage of ions were involved in such aggregates at high spacing, or N_{bb}. Random and periodic pendants at low N_{bb} also

dx.doi.org/10.1021/ja209142b | J. Am. Chem.Soc. 2012, 134, 574−587

formed large percolated aggregates. At higher N_{bb}, periodic pendants form roughly spherical, controlled size aggregates with liquid-like interaggregate order. These fit the physical picture of the YC or KT model of ionic aggregate morphology. The polymer backbone often bridges between aggregates or loops closely back within an aggregate, helping to set the interaggregate order. Adding randomness in the backbone spacing of charged beads disrupts this order, and random pendants' aggregates are larger, more variable in size, and stringlike rather than spherical.

All ionic aggregate morphologies yield an ionomer scattering peak. For precise pendants at high N_{bb} this corresponds to interaggregate order (and for these cases the ionomer peak is the most intense), but apparently even large percolated aggregates have mesoscale order within the aggregate on a similar length scale. For all types of architectures considered, increasing N_{bb} systematically moves the peak to lower wavevector, corresponding to longer length scales independent of changes in aggregate shape.

Our focus has been on ionic aggregate structure in coarse-grained ionomers of various architectures, and we have begun to study the detailed cluster and counterion dynamics in these systems. We expect to report insights into the mechanism of transport and which architectures may best facilitate counterion transport in a future publication. Further experimental studies are also underway. We hope to make further specific comparisons between experimental results on fully neutralized materials and our simulations.

■ ASSOCIATED CONTENT

Supporting Information

Table of additional data for the systems discussed above at σ_{ci} = 0.5 and graphs showing results of smaller scale simulations for periodic ionenes and pendants with σ_{ci} = 0.5 and 1.0 at N_{bb} = 3, 5, 7, and 9 and ε_r = 4, 6, 8, and 10. This material is available free of charge via the Internet at http://pubs.acs.org.

■ AUTHOR INFORMATION

Corresponding Author

lhall@sandia.gov; alfrisc@sandia.gov

Present Addresses

[⊥]DSM, Geleen, The Netherlands

[#]DuPont Experimental Station, Wilmington, DE

■ ACKNOWLEDGMENTS

We thank Frank van Swol for helpful discussions about the cluster analysis. This work was supported by the Sandia Laboratory Directed Research and Development Program. This work was also supported by the National Science Foundation Polymers Program, Grant DMR 1103858 (Seitz and Winey). K.L.O. and K.B.W. were supported by the National Science Foundation Grant DMR 0703261 and the Army Research Office award number W911NF-09-1-0290. This work was performed, in part, at the Center for Integrated Nanotechnologies, a U.S. Department of Energy, Office of Basic Energy Sciences user facility. Sandia National Laboratories is a multiprogram laboratory operated by Sandia Corporation, a Lockheed Martin Company, for the U.S. Department of Energy under Contract No. DE-AC04-94AL85000.

■ REFERENCES

(1) Eisenberg, A.; Kim, J.-S. *Introduction to Ionomers*; Wiley: New York, 1998.
(2) Yarusso, D. J.; Cooper, S. L. *Macromolecules* **1983**, *16*, 1871−1880.
(3) Laurer, J. H.; Winey, K. I. *Macromolecules* **1998**, *31*, 9106−9108.
(4) Seitz, M. E.; Chan, C. D.; Opper, K. L.; Baughman, T. W.; Wagener, K. B.; Winey, K. I. *J. Am. Chem. Soc.* **2010**, *132*, 8165−8174.
(5) Kinning, D. J.; Thomas, E. L. *Macromolecules* **1984**, *17*, 1712−1718.
(6) Winey, K. I.; Laurer, J. H.; Kirkmeyer, B. P. *Macromolecules* **2000**, *33*, 507−513.
(7) Kirkmeyer, B. P.; Weiss, R. A.; Winey, K. I. *J. Polym. Sci.: Polym. Phys.* **2001**, *39*, 477−483.
(8) Kirkmeyer, B. P.; Taubert, A.; Kim, J.-S.; Winey, K. I. *Macromolecules* **2002**, *35*, 2648−2653.
(9) Benetatos, N. M.; Winey, K. I. *J. Polym. Sci: Part B: Polym. Phys.* **2005**, *43*, 3549−3554.
(10) Batra, A.; Cohen, C.; Kim, H.; Winey, K. I.; Ando, N.; Gruner, S. M. *Macromolecules* **2006**, *39*, 1630−1638.
(11) Benetatos, N. M.; Heiney, P. A.; Winey, K. I. *Macromolecules* **2006**, *39*, 5174−5176.
(12) Benetatos, N. M.; Chan, C. D.; Winey, K. I. *Macromolecules* **2007**, *40*, 1081−1088.
(13) Ayyagari, C.; Bedrov, D.; Smith, G. D. *Polymer* **2004**, *45*, 4549−4558.
(14) Semenov, A. N.; Nyrkova, I. A.; Khokhlov, A. R. *Macromolecules* **1995**, *28*, 7491−7500.
(15) Nyrkova, I. A.; Khokhlov, A. R.; Doi, M. *Macromolecules* **1993**, *26*, 3601−3610.
(16) Kolbet, K. A.; Schweizer, K. S. *Macromolecules* **2000**, *33*, 1425−1442.
(17) Kolbet, K. A.; Schweizer, K. S. *Macromolecules* **2000**, *33*, 1443−1458.
(18) Kolbet, K. Ph.D. thesis, University of Illinois at Urbana-Champaign, 1999.
(19) Hickner, M. A. *Mater. Today* **2010**, *13*, 34−41.
(20) Elliott, J. A.; Paddison, S. J. *Phys. Chem. Chem. Phys.* **2007**, *9*, 2602−2618.
(21) Peckham, T.; Holdcroft, S. *Adv. Mater.* **2010**, *22*, 4667−4690.
(22) Allahyarov, E.; Taylor, P. L. *J. Chem. Phys.* **2007**, *127*, 154901.
(23) Goswami, M.; Kumar, S. K.; Bhattacharya, A.; Douglas, J. F. *Macromolecules* **2007**, *40*, 4113−4118.
(24) Wong, C.; Clarke, J. H. R. *J. Chem. Phys.* **2002**, *116*, 6795.
(25) Hall, L. M.; Stevens, M. J.; Frischknecht, A. L. *Phys. Rev. Lett.* **2011**, *106*, 127801.
(26) Baughman, T. W.; Chan, C. D.; Winey, K. I.; Wagener, K. B. *Macromolecules* **2007**, *40*, 6564−6571.
(27) http://www.datasqueezesoftware.com/
(28) Kremer, K.; Grest, G. S. *J. Chem. Phys.* **1990**, *92*, 5057.
(29) *Monte Carlo and Molecular Dynamics Simulations in Polymer Science*; Binder, K., Ed.; Oxford: New York, 1995.
(30) LAMMPS: Large-scale Atomic/Molecular Massively Parallel Simulator, http://lammps.sandia.gov
(31) Plimpton, S.; Pollock, R.; Stevens, M. *J. Comput. Phys.* **1995**, *117*, 1−19.
(32) Plimpton, S.; Pollock, R.; Stevens, M. Particle Mesh Ewald and rRESPA for Parallel Molecular Dynamics Simulations. *Proceedings of the 8th SIAM Conference on Parallel Processing for Scientific Computing*, Minneapolis, MN, 1997.
(33) Kamath, G.; Cao, F.; Potoff, J. J. *J. Phys. Chem. B* **2004**, *108*, 14130−14136.
(34) Hoy, R. S.; Foteinpoulou, K.; Kröger, M. *Phys. Rev. E* **2009**, *80*, 031803.
(35) VMD: Visual Molecular Dynamics, http://www.ks.uiuc.edu/Research/vmd/
(36) Humphrey, W.; Dalke, A.; Schulten, K. *J. Mol. Graphics* **1996**, *14*, 33−38.
(37) Stone, J. M.Sc. thesis, University of Missouri-Rolla, 1998.

(38) Theodorou, D. N.; Suter, U. W. *Macromolecules* **1985**, *18*, 1206−1214.
(39) Karayiannis, N. C.; Foteinopoulou, K.; Laso, M. *J. Chem. Phys.* **2009**, *130*, 164908.
(40) Fry, D.; Mohammad, A.; Chakrabarti, A.; Sorensen, C. M. *Langmuir* **2004**, *20*, 7871−7879.
(41) Khalatur, P. G.; Khokhlov, A. R.; Nyrkova, I. A.; Semenov, A. N. *Macromol. Theory Simul.* **1996**, *5*, 713−747.
(42) Datye, V. K.; Taylor, P. L. *Macromolecules* **1985**, *18*, 1479−1482.